

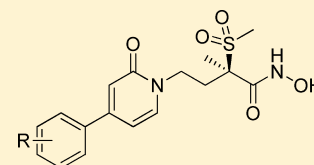
Pyridone Methylsulfone Hydroxamate LpxC Inhibitors for the Treatment of Serious Gram-Negative Infections

Justin I. Montgomery,^{*,†} Matthew F. Brown,[†] Usa Reilly,[†] Loren M. Price,[†] Joseph A. Abramite,[†] Joel Arcari,[†] Rose Barham,[†] Ye Che,[‡] Jinshan Michael Chen,[†] Seung Won Chung,[†] Elizabeth M. Collantes,[‡] Charlene Desbonnet,[§] Matthew Doroski,[†] Jonathan Doty,[†] Juntyma J. Engtrakul,^{||} Thomas M. Harris,[†] Michael Huband,[§] John D. Knafels,[⊥] Karen L. Leach,[§] Shenping Liu,[⊥] Anthony Marfat,[†] Laura McAllister,[†] Eric McElroy,[†] Carol A. Menard,[#] Mark Mitton-Fry,[†] Lisa Mullins,[§] Mark C. Noe,[†] John O'Donnell,[§] Robert Oliver,[†] Joseph Penzien,[§] Mark Plummer,[†] Veerabahu Shanmugasundaram,[‡] Christy Thoma,[§] Andrew P. Tomaras,[§] Daniel P. Uccello,[†] Alfin Vaz,^{||} and Donn G. Wishka[†]

[†]Worldwide Medicinal Chemistry, [‡]Computational Chemistry, [§]Antibacterials Research Unit, ^{||}Drug Metabolism, [⊥]Structural Biology, [#]Primary Pharmacology, Pfizer Worldwide Research and Development, 445 Eastern Point Road, Groton, Connecticut 06340, United States

S Supporting Information

ABSTRACT: The synthesis and biological activity of a new series of LpxC inhibitors represented by pyridone methylsulfone hydroxamate **2a** is presented. Members of this series have improved solubility and free fraction when compared to compounds in the previously described biphenyl methylsulfone hydroxamate series, and they maintain superior Gram-negative antibacterial activity to comparator agents.



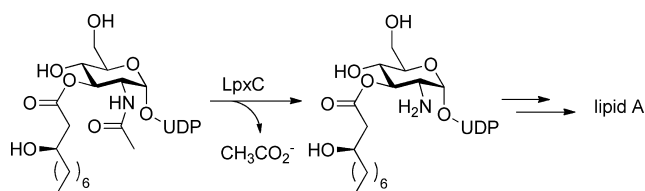
■ INTRODUCTION

As the antibiotic pipeline continues to decline, considerable concern has developed around growing resistance in bacterial species responsible for hospital-acquired infections.¹ The so-called “ESKAPE” pathogens,² *Enterococcus faecium*, *Staphylococcus aureus*, *Klebsiella pneumoniae*, *Acinetobacter baumannii*, *Pseudomonas aeruginosa*, and *Enterobacter* species, account for a large proportion of nosocomial infections, and while substantial progress toward the treatment of the resistant Gram-positive ESKAPE organisms has been achieved, few, or in many cases no, drugs exist for the multidrug resistant Gram-negatives (KAPE),³ creating a high medical need for new agents that can overcome these “bad bugs”.⁴ LpxC (UDP-3-O-(R-3-hydroxymyristoyl)-N-acetylglucosamine deacetylase) is a metallo-enzyme that catalyzes the first committed step in the biosynthesis of lipid A, an essential component of the outer membrane of Gram-negative bacteria (Scheme 1).⁵ LpxC is an attractive

antibacterial target as there is no human homologue and it is highly conserved in Gram-negative bacteria. As no inhibitors of LpxC have been approved to date, antibiotics from this new chemical class would likely overcome pre-existing class-specific mechanisms of resistance such as extended-spectrum β -lactamases (ESBLs),⁶ *Klebsiella pneumoniae* carbapenemases (KPCs),⁷ and the recently described New Delhi metallo- β -lactamase (NDM-1).⁸

Various small-molecule LpxC inhibitors have been disclosed in patents and journal articles over the last two decades,⁹ but to our knowledge, none have reached the clinic. An earlier report from our laboratories describes biphenyl methylsulfone hydroxamate inhibitors with impressive activity and spectrum.¹⁰ Unfortunately, the series suffered from high clearance, high protein binding, and low solubility, and had high human efficacious dose projections. In a typical medicinal chemistry program targeting oral delivery of drug, free fraction (f_u) has little to no effect on the free concentration of drug achieved at the target site, as clearance generally goes up as free levels increase,¹¹ however, an exception exists in the case of high clearance drugs delivered intravenously.¹² When these conditions exist, free AUC is directly proportional to f_u and f_u has a dramatic effect on dose predictions. For these reasons, we set out to both improve solubility and increase f_u in our series to consequently increase our ability to deliver more drug in an acceptable volume for iv delivery and improve free exposure

Scheme 1. Deacetylation of UDP-3-O-(R-3-hydroxymyristoyl)-N-acetylglucosamine Catalyzed by LpxC, the First Committed Step in the Biosynthesis of Lipid A



Received: November 4, 2011

Published: January 18, 2012

respectively, all while maintaining the excellent antibacterial activity and spectrum of the previously described biphenyl methyl sulfones. Herein, we describe efforts to replace the central phenyl ring in biphenyl methylsulfone hydroxamate **1** (Figure 1) with more polar groups culminating in the discovery

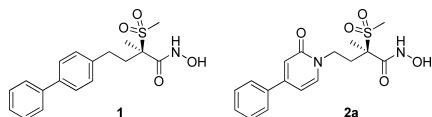


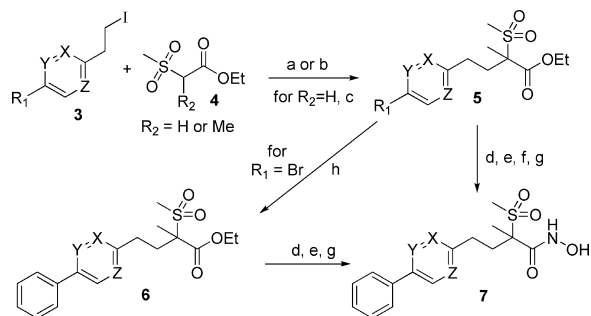
Figure 1. Methylsulfone hydroxamate LpxC inhibitors.

of pyridone **2a** as well as the SAR and antibacterial spectrum of the pyridone methylsulfone hydroxamate series.

CHEMISTRY

The synthesis of the hydroxamic acids **7** (Scheme 2) began with base promoted alkylation of ethyl esters (**4**) with the

Scheme 2. Synthesis of Methylsulfone Hydroxamic Acids^{a,b}



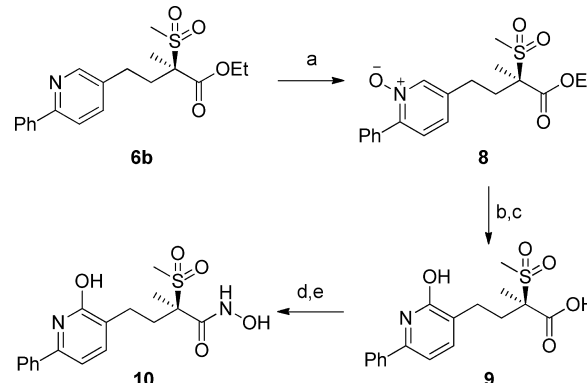
^aRacemic synthesis shown: separation of enantiomers can be performed at the hydroxamic acid (**7**) stage using chiral chromatography.

^bReagents and condition: (a) NaH, DMF; (b) Cs₂CO₃, DMF 50 °C; (c) MeI, Cs₂CO₃, DMF; (d) LiOH, THF, H₂O; (e) method A, CDI, DMF, THPONH₂; method B, (1) CDMT, NMM, 2-MeTHF, (2) THPONH₂; method C, EDC, HOBT, THPONH₂; (f) method A, Silicat Pd-Dppf, K₂CO₃, EtOH:H₂O (9:1), 70 °C; method B, PhB(OH)₂, Pd EnCat, K₂CO₃, EtOH:H₂O (9:1), 70 °C; (g) HCl (h) PhB(OH)₂, Pd(dppf)Cl₂, K₃PO₄, 1,4-dioxane.

appropriate alkyl iodides **3**, which were readily synthesized from the corresponding alcohols. When ethyl (methylsulfonyl)acetate was used in the initial alkylation, a second alkylation using methyl iodide was performed to afford the corresponding ethyl esters **5**. The aryl bromides **5** (R₁ = Br) were converted to the corresponding hydroxamic acids **7** via saponification of the ethyl ester, amidation of the free acid with *O*-(tetrahydro-2*H*-pyran-2-yl)hydroxylamine (THPONH₂) to afford the protected hydroxamic acid, Suzuki–Miyaura cross coupling using phenylboronic acid, and acid hydrolysis to reveal the free hydroxamate. Alternatively, the Suzuki–Miyaura cross coupling can be performed directly on ethyl esters **5** to provide coupled products **6**, followed by the same end-game steps leading to hydroxamic acids **7**. When desired, the two enantiomers of methylsulfone hydroxamates **7** can easily be separated at this stage through the use of chiral chromatography.

Compound **10** (Scheme 3) was obtained via a *m*CPBA oxidation of the pyridyl intermediate **6a** to afford the *N*-oxide **8**, which rearranged in refluxing acetic acid to a hydroxy pyridine. Saponification gave the free acid **9**, which was then converted to the hydroxamic acid **10** as previously described.

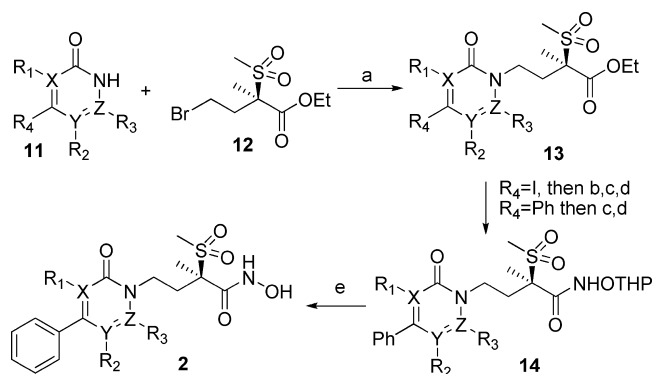
Scheme 3. Synthesis of Compound 10^a



^aReagents and conditions: (a) *m*CPBA, DCM; (b) AcOH, Δ; (c) LiOH, THF, MeOH, H₂O; (d) amide coupling w/THPONH₂, THPONH₂, HATU, DIPEA, DMF; (e) THP deprotection; HCl, DCM, MeOH.

Various pyridone analogues were synthesized to explore the SAR around the core of the hydroxamic acids **2** (Scheme 4).

Scheme 4. Synthesis of Modified Pyridone Methylsulfone Hydroxamic Acids^a

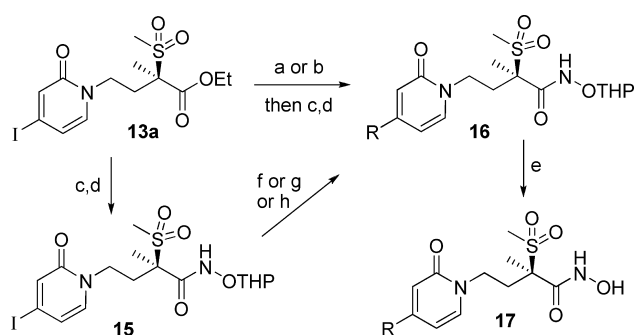


^aReagents and conditions: (a) Alkylation: method A, Cs₂CO₃, THF, 65 °C; method B, K₂CO₃, DMF, rt; method C, K₂CO₃, TBAB, ACN, Δ. (b) Suzuki–Miyaura coupling, PhB(OH)₂, Pd(II) EnCat, K₂CO₃, EtOH:H₂O (9:1). (c) Saponification: method A, LiOH, THF, MeOH, H₂O; method B, KOH. (d) Amide coupling w/THPONH₂: method A, (1) HOBT, DIPEA (TEA), DCM (DMF), (2) THPONH₂, EDCI; method B, (1) CDMT, NMM, 2-MeTHF, (2) THPONH₂. (e) THP deprotection: method A, PPTS, EtOH; method B, HCl.

Synthesis of these analogues required base mediated alkylation of the corresponding free pyridones **11** with the *R*-enantiomer of alkyl bromide **12** to afford ethyl ester **13**. A Suzuki–Miyaura cross coupling was performed, when necessary, to afford the desired phenyl analogue, which was converted to the hydroxamic acids **2** via the previously described sequence involving saponification, amide coupling, and acid deprotection.

Intermediate **16** was synthesized via two pathways (Scheme 5). The ethyl ester **13a** was readily elaborated through metal-mediated coupling reactions (Suzuki–Miyaura or Negishi), followed by standard protocols for the conversion of the ester to the THP protected hydroxamic acid **16**. Alternatively, intermediate **15** was efficiently synthesized from the ethyl ester **13a** and was primed for the two-step analoguing sequence to the desired hydroxamic acids **17**. Metal-mediated coupling (Suzuki–Miyaura, Negishi, Sonogashira, or Grignard) of **15** to the

Scheme 5. Synthesis of Substituted Pyridone Methylsulfone Hydroxamic Acids^a

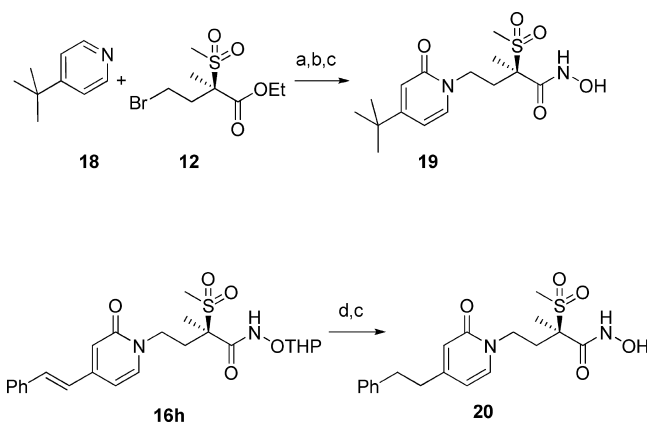


^aReagents and conditions: (a) Suzuki–Miyaura coupling: $\text{RB}(\text{OC}(\text{CH}_3)_2)_2$, $\text{Pd}(\text{dppf})\text{Cl}_2$, K_3PO_4 , 2-MeTHF. (b) Negishi coupling: RZnBr , $\text{Pd}(\text{PPh}_3)_4$, THF. (c) Saponification: LiOH . (d) Amide coupling w/THPONH₂: (1) CDMT, NMM, 2-MeTHF; (2) THPONH₂. (e) THP deprotection: method A, PPTS, EtOH; method B, HCl. (f) Suzuki–Miyaura coupling: method A, $\text{RB}(\text{OR}')_2$ or $(\text{MeBO})_3$, $\text{Pd}(\text{PPh}_3)_4$, K_2CO_3 , 1,4-dioxane, H₂O, 80 °C; method B, $\text{RB}(\text{OR}')_2$, Pd Encat, K_2CO_3 , EtOH, H₂O, 70 °C; method C, $\text{RB}(\text{OR}')_2$, SiliaCat DPP-Pd, K_2CO_3 , EtOH, H₂O, 70 °C; $\text{RB}(\text{OR}')_2$, $\text{Pd}(\text{dppf})\text{Cl}_2$, K_2CO_3 , 1,4-dioxane, H₂O, 80 °C. (g) Sonogashira coupling: PhCCH , $\text{Pd}(\text{PPh}_3)_4$, CuI, DIPEA, THF, rt. (h) Grignard reaction: $\text{C}_6\text{H}_{11}\text{MgBr}$, $\text{CuBr}\cdot\text{Me}_2\text{S}$, THF, -78 °C to rt.

appropriate boronate, zincate, acetylene, or Grignard species afforded the corresponding THP protected hydroxamic acids **16**. Acid-promoted THP deprotection then gave the desired hydroxamic acids **17**.

As shown in Scheme 6, hydroxamic acid **19** was prepared via alkylative-oxidation of *t*-butylpyridine and the alkyl bromide **12**

Scheme 6. Additional Transformations Not Covered by Previous Schemes^a



^aReagents and conditions: (a) (1) 100 °C, 1 h; (2) 1 N aq NaOH, $\text{K}_3\text{Fe}(\text{CN})_6$, 100 °C to rt. (b) Amide coupling w/THPONH₂: method A, (1) CDMT, NMM, 2-MeTHF, (2) THPONH₂; method B, THPONH₂, HATU, DIPEA, DMF. (c) THP deprotection: method A, TFA, DMSO; method B, HCl, DCM, MeOH. (d) C_6H_8 , 10% Pd/C, EtOH, rt.

in the presence of potassium ferricyanide (III) and 1 N aq NaOH, followed by THPONH₂ amidation and THP deprotection. Alkene **16h** was converted to the alkane **20** via transfer hydrogenation followed by acidic THP deprotection.

RESULTS AND DISCUSSION

In the following tables, *Pseudomonas aeruginosa* (Pae) enzyme potency (Pae IC₅₀) as well as two minimum inhibitory

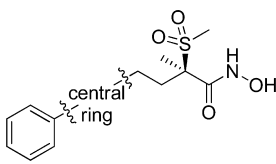
concentrations (MICs) are presented. Strain PA3919 is a Pae strain lacking major efflux pumps ($\Delta(\text{mexAB-OprM})\Delta(\text{mexXY})\Delta(\text{MexZ})$), while PA01 is a fully efflux-competent wild type Pae strain.

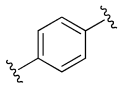
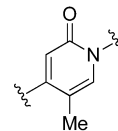
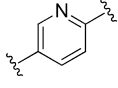
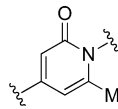
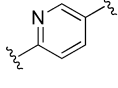
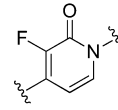
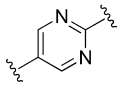
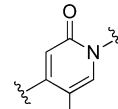
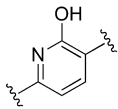
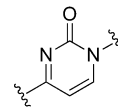
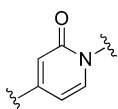
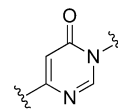
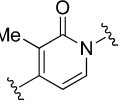
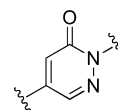
As solubility and f_u are generally correlated with polarity,¹³ we began by introducing heteroatom substitutions within the central ring (Table 1) with the goal of increasing polarity without sacrificing activity. Pyridine **7a** was less active than phenyl analogue **1** by about 9-fold in enzyme potency and 4–5 dilutions in whole cell activity. Moving the nitrogen atom over one position as in pyridine **7b** slightly lowered activity; however, introducing polarity on both sides of the central ring as in pyrimidine **7c** resulted in a larger reduction of both enzyme and wild type Pae whole cell activity (PA01). C-Linked pyridone **10** was only moderately active, but N-linked pyridone **2a** maintained favorable potency (Pae IC₅₀ = 3.6 nM) and MICs (PA01 = 0.5 μg/mL). In addition, cLogD was reduced by 1.7 units (2.2 for **1**, 0.5 for **2a**) with the phenyl-to-pyridone substitution. The three monomethyl analogues **2b**, **2c**, and **2d** were investigated, and while all had measurable activity, the 3-methyl analogue **2b** was superior and was similar in activity to the parent pyridone **2a**. Fluorine was also tolerated in the 3- (**2e**) and 5-positions (**2f**), and in these analogues, PA01 activity was similar to analogue **2a**. Finally, substituting in a second nitrogen atom in the 3- (**2g**) or 6-position (**2i**) led to a substantial loss of activity, but pyrimidinone **2h** maintained high antibacterial activity, and cLogP in this analogue was further reduced to -1.4.

The cocrystal structure of pyridone **2a** in Pae LpxC enzyme (Figure 2) was solved, revealing binding similar to that seen for hydroxamate methylsulfone headgroup containing biphenyl compounds.¹⁰ Data collection and refinement statistics for the costructure are presented in Table 2. The pyridone oxygen oriented toward methionine 62 in a relatively hydrophobic pocket rather than binding in the opposite orientation to interact with threonine 190, which modeling had suggested was a possibility, but this alternate binding mode would have disrupted the H-bond between the hydroxamate carbonyl and threonine 190. Key additional interactions of **2a** with the LpxC enzyme include the hydroxamate zinc binding motif, the sulfone–lysine 238 interaction, the positioning of the sulfone methyl group in a hydrophobic pocket, and multiple hydrophobic contacts at the tail end of the molecule. As in the biphenyl series, a good opportunity for optimizing potency and properties was through modification of the pendant phenyl group.

Having discovered a more polar, but equally active replacement for the central phenyl ring in **1**, we set out to study the SAR around the terminal ring in pyridone **2a** (Table 3). Replacing the phenyl ring with various pyridines (**17a–c**) led to substantial loss of activity, highlighting the importance of maintaining hydrophobic contacts in this area of the enzyme. 4-Pyridine **17c**, in which the polarity is placed toward the exit of the hydrophobic tunnel, was the most potent pyridine at 39 nM, but the 2-pyridine analogue **17a** had better wild type Pae activity. Surprisingly, pyridine **17d** with an effective methoxy substitution para to the pyridone ring connection, was quite active, with 6.4 nM potency and a 2 μg/mL wild type Pae MIC. Unfortunately, its Gram-negative spectrum was narrower than pyridone **2a** (vide infra, Table 7). Removing the terminal phenyl completely and replacing it with a methyl group (**17e**) was detrimental to enzyme potency but did not obliterate whole-cell activity completely. Increasing the size of

Table 1. Central Ring SAR



cmpd	central ring	Pae IC50 (nM)	MICs (ug/mL) PA3919	PA01	cmpd	central ring	Pae IC50 (nM)	MICs (ug/mL) PA3919	PA01
1		1.4 ± 0.7	0.008	0.125	2c		30 ± 18	0.125	8
7a		13 ± 2 ^a	0.125 ^a	4 ^a	2d		22 ± 5	0.125	4
7b		49 ± 24 ^a	0.25 ^a	8 ^a	2e		4.9 ± 0.9	0.015	1
7c		>100 ^a	4 ^a	>64 ^a	2f		2.3 ± 1.2	0.015	0.5
10		53 ^{a,b}	1 ^a	32 ^a	2g		57 ± 27	0.5	16
2a		3.6 ± 0.8	0.06	0.5	2h		8.5 ± 1.5	0.03	1
2b		6.7 ± 0.5	0.015	0.5	2i		>72 ± 29	1	32

^aBiological data for racemic compound. ^b_n = 1 IC50 data.

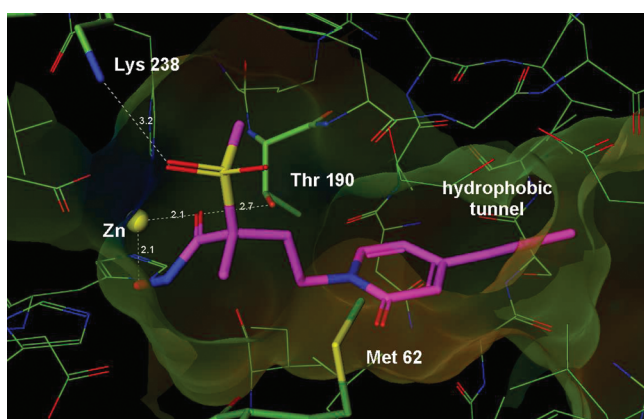


Figure 2. Co-crystal structure of pyridone **2a** in complex with *Pseudomonas aeruginosa* LpxC (RCSB PDB ID 3UHM).

the alkyl group to *tert*-butyl (**19**) restored enzyme activity to double digit nM numbers, suggesting beneficial hydrophobic interactions in this area. The cyclohexyl analogue **17f** was less active than phenyl pyridone **2a**, but the introduction of a single unsaturation in cyclohexenyl pyridone **17g** completely restored that activity. The phenyl alkyne substituent was quite active in

the pyridone series (**17h**), but upon incubation of this analogue with glutathione, we saw covalent modification of the alkyne, and the series was deprioritized. Alkyne replacements such as alkene **17i** and alkane **20** were also investigated, but these isosteres dropped off in activity, especially against tougher Pae stains in our MIC90 panel (data not shown).

Although over 500 pyridone analogues with substituted phenyl groups were synthesized and characterized, only a selection of molecules that illustrate key SAR points and/or represent the most active analogues are presented in Table 4. Introducing a single fluorine on the phenyl ring in any position (**17j–l**) led to slightly improved activity over phenyl pyridone **2a** and difluoro analogues (**17m–o**) had activity very similar to **2a**. However, introducing 2,6-dimethyl substitution (**17p**) led to a substantial loss of activity, illustrating that the hydrophobic tunnel cannot comfortably accommodate these larger groups. 3,5-Dimethyl analogue **17q**'s activity was closer to the parent compound **2a** but still fell off slightly. In addition, mid-sized groups such as methoxy in the ortho position (**17r**) led to loss of activity relative to analogue **2a**. Methoxy in the meta position as in **17s** was about equally active to phenyl pyridone **2a**. Excitingly, *para*-methoxy derivative **17t** was significantly more active than **2a** with wild type Pae MIC = 0.125 μg/mL. Combining methoxy and fluorine substituents led to a number

Table 2. Data Collection and Refinement Statistics (RCSB PDB ID 3UHM)

Data Collection	
space group	$P2_1$
cell dimensions	
a, b, c (Å)	34.14, 80.97, 49.78
α, β, γ (deg)	90, 95.5, 90
resolution (Å) ^a	50.0–1.5 (1.53–1.5)
R_{merge}	0.049 (0.059)
I/σ	24.1 (22.7)
completeness (%)	87.3(84.1)
redundancy	3.4 (2.5)
Refinement	
resolution (Å)	50–1.5 (1.54–1.50)
no. refls	37,590 (2,757)
$R_{\text{work}}/R_{\text{free}}$	0.175 (0.137)/0.208 (0.193)
no. atoms	
protein	2,351
ligand/ion	34
water	242
rms deviations	
bond lengths (Å)	0.010
bond angles (deg)	1.07

^aStatistics in the highest resolution shell are shown in parentheses. Crystal diffracted to 1.26 Å, but was limited to 1.5 Å for completeness.

of quite active analogues (17u, 17v, 17w). Chlorine in the para position was also found to increase potency as illustrated by analogue 17x. Trifluoro analogue 17y was slightly less active than 17x, but switching to a *para* chloro substituent (17z) resulted in one of our most active analogues with a 0.52 nM Pae LpxC IC₅₀. Naphthyl analogue 17aa picked up a little activity over 2a but at the expense of increased cLogP (~1.2 units difference). A number of quite active analogues were found by adding a third ring (a heteroaromatic) to the para position of the pyridone phenyl ring (17bb–17hh). Of particular note are methoxy pyrimidine 17ee and various

5-membered heterocyclic analogues 17ff, 17gg, and 17hh, all of which had wild type Pae MICs of 0.25 μg/mL.

While searching for highly active LpxC inhibitors with more polarity than biphenyl methylsulfone 1, we were continuously measuring solubility and free fraction to make sure improvements were also made in these properties (Table 5). Aqueous thermodynamic solubility (from crystalline solid forms) was measured at three different pH levels: (1) pH 3, where the hydroxamate is fully protonated, providing a measure of intrinsic solubility, (2) pH 7.4, physiological conditions, and (3) pH 9, our upper limit for IV formulation/delivery and a pH where the hydroxamate is partially ionized. For biphenyl analogue 1, we found relatively low single digit μg/mL solubilities at low and neutral pH, but a significant increase at pH 9 to 260 μg/mL. Pyridone 2a had dramatically higher solubility at all measured pH's and over 16 mg/mL solubility at pH 9, which surpassed our target of 5 mg/mL for iv formulation. The more active pyridone analogue 17v, with additional polarity on the phenyl ring had intrinsic solubility of 82 μg/mL and ≥14 mg/mL at pH 9, but some of these solubility gains were lost in the three-ring analogues exemplified by 17hh, where solubility was only ~3 mg/mL at pH 9 (still ~10× greater than biphenyl analogue 1 at the same pH).

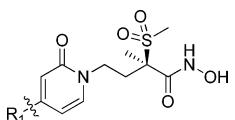
Free fraction in rat and human plasma was measured using equilibrium dialysis. Compound 1 was only 2% free in human plasma. Fortunately, the pyridones demonstrated much lower protein binding and were generally between 10% and 35% free. Parent pyridone 2a was 28% free in rat plasma but only 14% free in human plasma, while three-ring triazole 17hh was more free in human plasma. Analogue 17v was one of our best compounds in terms of free fraction, with >30% free in both species. Figure 3 is a plot of free fraction vs cLogD_{7.4} for multiple compounds (of varying activity) in the pyridone methylsulfone hydroxamate series (green stars) and biphenyl methylsulfone hydroxamate¹⁰ series (yellow circles). The blue shading shows the optimal cLogD_{7.4} range for both achieving good MICs (data not shown) and acceptable free fraction,

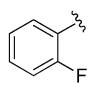
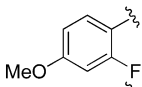
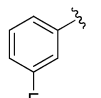
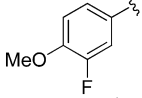
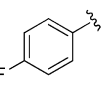
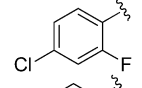
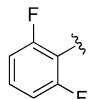
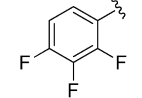
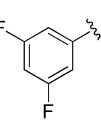
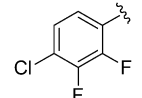
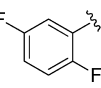
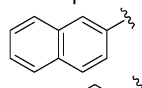
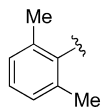
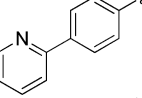
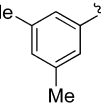
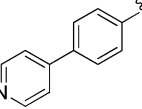
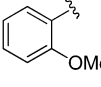
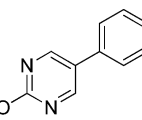
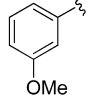
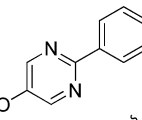
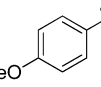
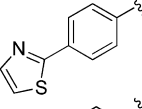
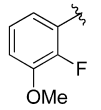
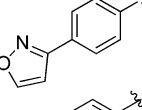
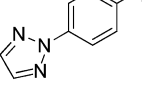
Table 3. Pyridone Terminal SAR (Non-phenyl)

cmpd	R ¹	Pae IC50 (nM)	MICs (ug/mL)		cmpd	R ¹	Pae IC50 (nM)	MICs (ug/mL)	
			PA3919	PA01				PA3919	PA01
17a		60 ± 28	0.25	4	17f		11 ± 3 ^a	0.06 ^a	2 ^a
17b		>100	2	>64	17g		4.1 ± 1.3	0.03	0.5
17c		39 ± 8	0.5	32	17h		1.8 ± 0.1	0.015	0.25
17d		6.4 ± 1.7	0.06	2	17i		3.2 ± 0.7	0.03	0.5
17e		>100	8	64	20		6.0 ± 1.0	0.03	2
19		69 ± 30	0.25	8					

^aBiological data for racemic compound.

Table 4. Pyridone Terminal SAR (Phenyl)



compd	R ¹	Pae IC ₅₀ (nM)	MICs (ug/mL)		compd	R ¹	Pae IC ₅₀ (nM)	MICs (ug/mL)	
			PA3919	PA01				PA3919	PA01
17j		2.2 ± 0.6	0.015	0.25	17v		1.1 ± 0.5	0.008	0.125
17k		3.0 ± 1.4	0.015	0.5	17w		2.0 ± 0.8	0.03	0.5
17l		2.9 ± 1.1	0.008	0.25	17x		1.0 ± 0.6	0.008	0.125
17m		4.8 ± 1.0	0.03	0.5	17y		1.5 ± 0.2	0.015	0.25
17n		3.9 ± 1.7	0.03	1	17z		0.52 ± 0.39	0.008	0.125
17o		4.4 ± 2.3	0.03	1	17aa		1.2 ^b	0.008	0.125
17p		>87 ± 15	2	64	17bb		1.3 ± 0.6	0.015	0.5
17q		5.3 ± 1.9	0.125	2	17cc		1.2 ± 0.2	0.03	0.5
17r		12 ± 2	0.125	4	17dd		2.0 ± 1.0	0.03	0.5
17s		3.7 ± 1.2	0.03	1	17ee		1.2 ± 0.1	0.03	0.25
17t		2.6 ± 0.8	0.008	0.125	17ff		1.1 ± 0.6	0.015	0.25
17u		1.8 ± 0.2	0.015	0.5	17gg		1.1 ± 0.3	0.015	0.25
					17hh		0.53 ± 0.12	0.015	0.25

^b_n = 1 IC₅₀ data.

Table 5. Properties, Solubility, And Free Fraction of Select Analogues

compd	MW	cLogP	cLogD _{7.4}	thermosol μg/mL			rat <i>f_u</i>	human <i>f_u</i>
				pH 3	pH 7.4	pH 9		
1	347.4	1.93	2.17	7.3	3.9	260	0.026	0.023
2a	364.4	-0.80	0.51	410	480	>16000	0.28	0.14
17v	412.4	-0.57	0.56	82	130	>14000	0.32	0.31
17hh	431.5	-0.60	0.09	3.3	9.2	2740	0.13	0.25

and one can readily see the inherent f_u advantage of the pyridone series in this polarity range.

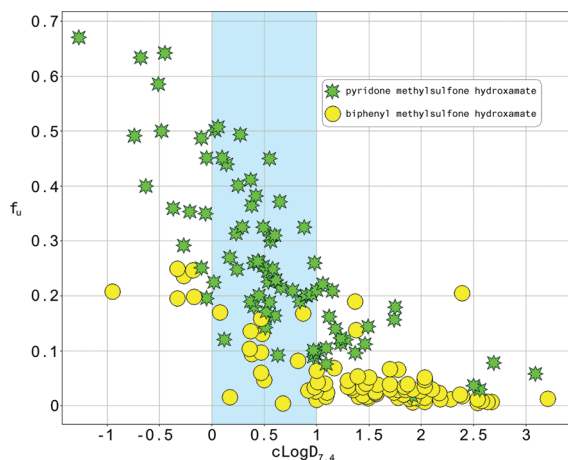


Figure 3. Plot of human free fraction (f_u) vs $c\text{LogD}_{7.4}$ for two series.

Table 6 contains rat PK for various methylsulfone analogues. High clearance was observed for all compounds with the

Table 6. Rat PK for Select Compounds

compd	dose (mg/kg)	CI (mL/min/kg)	Vdss (L/kg)	$T_{1/2}$ (h)	AUC ($\mu\text{g}\cdot\text{h}/\text{mL}$)	free AUC ($\mu\text{g}\cdot\text{h}/\text{mL}$)
1	10	57	3.8	3.2	2.9	0.075
28	10	78	1.7	1.0	2.1	0.59
17v	10	72	1.7	1.4	2.3	0.74
17hh	10	32	0.92	0.94	5.2	0.68

exception of triazole **17hh** (32 mL/min/kg). Total AUC was relatively consistent for the original biphenyl lead **1** (2.9 $\mu\text{g}\cdot\text{h}/\text{mL}$) and pyridone comparators **2a**, **17v**, and **17hh** (2.1 to 5.2 $\mu\text{g}\cdot\text{h}/\text{mL}$), but as the efficacy of these LpxC inhibitors is related to free AUC, an order of magnitude advantage exists for the pyridones over biphenyl analogue **1**, which, as noted earlier, directly translates into lower human dose predictions (unpublished results).

Table 7 presents MIC90 values for multiple species of Gram-negative bacteria for various methylsulfone hydroxamates in comparison to biphenyl methylsulfone hydroxamate **1** and approved agents. For *Pseudomonas aeruginosa* (Pae), all of the novel LpxC inhibitors are superior to the marketed agents, ciprofloxacin and aztreonam. In comparing compounds with modification at the central ring and a terminal phenyl ring, pyridone **2a** has a better Pae MIC90 than fluoropyridone **2f** and pyrimidinone **2h**. Compound **17d** with a terminal methoxy substituted pyridine ring, drops off significantly with a Pae MIC90 of 16 $\mu\text{g}/\text{mL}$. Alkyne **17h** is equally active to pyridone **2a**, but substituted aryl pyridones **17v**, **17x**, **17y**, **17aa**, and **17hh** have Pae MIC90 = 1 $\mu\text{g}/\text{mL}$. The most active analogue for Pae was trihalogen substituted pyridone **17z** with an impressive MIC90 of 0.25 $\mu\text{g}/\text{mL}$ for the 22 strains tested. For *Escherichia coli* (Eco), pyridone **2a** had a relatively weak MIC90 of 8 $\mu\text{g}/\text{mL}$, but substitution of the terminal aromatic ring resulted in multiple analogues with very low MIC90s of <0.5 $\mu\text{g}/\text{mL}$. Similarly, for *Klebsiella pneumoniae* (Kpn), aryl ring substitution led to quite low MIC90s. Amazingly, three-ring triazole analogue **17hh** had a Kpn MIC90 of only 0.125 $\mu\text{g}/\text{mL}$. None of the new analogues were particularly active for

Table 7. MIC90s of Select Analogues and Control Compounds

compd	species ^a (n), MIC90s ($\mu\text{g}/\text{mL}$)					
	Pae (22)	Eco (11)	Kpn (22)	Asp (11)	Eae (11)	Cfr (11)
ciprofloxacin	64	>64	64	64	1	32
aztreonam	64	>64	>64	32	32	>64
1	4	2	16	32	4	8
2a	2	8	16	32	16	8
2f	4	4	8	32	8	8
2h	4	8	16	64	16	16
17d	16	8	32	>64	32	16
17h	2	0.06	0.5	>64	0.25	0.125
17v	1	0.25	0.5	>64	0.5	0.5
17x	1	0.125	1	64	0.5	0.5
17y	1	0.5	2	>64	1	0.5
17z	0.25	0.06	0.5	>64	0.25	0.25
17aa	1	0.06	0.5	>64	0.25	0.125
17hh	1	0.06	0.125	64	0.125	0.125

^aPae, *Pseudomonas aeruginosa*; Eco, *Escherichia coli*; Kpn, *Klebsiella pneumoniae*; Asp, *Acinetobacter* spp.; Eae, *Enterobacter aerogenes*; Cfr, *Citrobacter freundii*.

Acinetobacter spp. (Asp), which was not surprising given the drop in LpxC enzyme potency we observe when comparing *Acinetobacter baumannii* IC₅₀s to Pae IC₅₀s (data not shown). Like Pae, Eco, and Kpn, *Enterobacter aerogenes* (Eae) and *Citrobacter freundii* (Cfr) MIC90s were quite good (generally <1 $\mu\text{g}/\text{mL}$) for the more active pyridone analogues, clearly differentiating these new LpxC inhibitors from the marketed comparators.

CONCLUSION

Efforts to improve on the previously reported LpxC inhibitor **1** which suffered from low solubility and high protein binding resulted in the identification of a pyridone series of LpxC inhibitors with excellent Gram-negative antibacterial activity, improved solubility, and increased free fraction. Many of these novel compounds have MIC90s of ≤ 1 $\mu\text{g}/\text{mL}$ for multiple species and have met our targets for solubility and free fraction, which will enable us to achieve the required exposure to determine a relevant therapeutic index. The results of further in vivo experiments will be reported in due course.

EXPERIMENTAL SECTION

LpxC Enzyme Assay. The assay measures the enzymatic deacetylation of the synthetic lipid substrate UDP-3-O-(R-hydroxydecanoyl)-N-acetylglucosamine by mass spectrometry using a computer-controlled fluidic system combined with a triple quadrupole mass spectrometer (BioTrove RapidFire) and is similar to that reported by Langsdorf et al.¹⁴ The enzyme assay was conducted in 384-well polypropylene plates (Thermo no. 4312) in a total volume of 50 μL containing 100 pM purified *Pseudomonas aeruginosa* LpxC enzyme. The enzyme was expressed in *E. coli* and purified from cell lysates using a method based on a published protocol.¹⁵ Briefly, cell paste was resuspended in buffer containing 10 mM sodium phosphate, pH 7.0, 0.1 mM zinc chloride, and 10 mM magnesium chloride, in addition to Benzonase and EDTA-free protease inhibitor tablets. Cells were lysed by passing through a microfluidizer, then spun at 4500g for 1 h. The resulting supernatant was purified on a DEAE-Sepharose column, using a 0–150 mM NaCl gradient. Fractions containing the LpxC protein were pooled, concentrated, and purified on a Superdex 200 gel filtration column. The purified LpxC protein was stored at -80 $^{\circ}\text{C}$ until use. The substrate buffer contained 100 mM Na_2PO_4 , 1 mg/mL bovine serum albumin, pH 7.0. The enzyme buffer contained 5 mM Na_2PO_4 and 1.5 mg/mL bovine serum albumin, pH 7.5.

Compounds (5 μL in 100% DMSO; compound final concentration range 100 μM to 1.0 pM) were preincubated with 20 μL of LpxC enzyme for 30 min at room temperature. The substrate UDP-3-O-(R-hydroxydecanoyl)-N-acetylglucosamine, which was obtained from Alberta Research Council (Alberta, Canada), was added to initiate the assay, 25 μL at 1.0 μM (final concentration 0.5 μM). Assay plates were sealed, incubated at room temperature for 60 min, and the reaction stopped by the addition of 10 μL of 1 N hydrochloric acid. The plates were read on the BioTrove RapidFire with mass spec detection, and the product and substrate peak areas were determined. A percent substrate conversion was calculated in Microsoft Excel. The calculated values were entered into an internally developed (within Pfizer) data analysis program (Sights), and curves were drawn based on the percent substrate conversion data points. An 11-point dose response was plotted and IC_{50} determinations were made by that software package. Unless otherwise noted, IC_{50} values are reported as the average of 3 or more runs (n) \pm the standard deviation.

Antimicrobial Susceptibility Testing. The minimum inhibitory concentration (MIC) values were determined using the broth micro-dilution protocol according to the methods of the Clinical and Laboratory Standards Institute (CLSI).

Inoculum Preparation and Direct Colony Suspension. Bacterial strains were grown on Tryptic Soy Agar with 5% Sheep Blood for 24 h prior to testing. Colonies of strains were suspended into sterile saline until a turbidity standard of 0.5 McFarland was achieved (approximately 1×10^8 CFU/mL). This suspension was diluted 1:400 in Mueller–Hinton broth (2.5×10^5 CFU/mL).

Drug Dilution Tray Preparation. Compounds are diluted in appropriate solvent to 2200 $\mu\text{g}/\text{mL}$. The microbroth dilution stock plates were prepared in 2-fold dilution series, 64 to 0.06 μg drug/mL (high dilution series) and 0.25 to 0.00025 μg drug/mL (low dilution series). For tube 1 of the high dilution series, 200 μL of the 2220 $\mu\text{g}/\text{mL}$ stock was added to duplicate wells of a 96-well microtiter plate. For tube 1 of the low concentration series, 200 μL of an 8.33 $\mu\text{g}/\text{mL}$ stock was added to duplicate rows of a 96-well microtiter plate. Serial 2-fold decremental dilutions were made using a BioMek FX robot (Beckman Coulter Inc., Fullerton, California) with 10 of the remaining 11 wells, each of which contained 100 μL of the appropriate solvent/diluent. Row 12 contained solvent/diluent only and served as the control. Daughter plates were spotted (3.0 $\mu\text{L}/\text{well}$) from the stock plates listed above using the BioMek FX robot, yielding the final concentration of drug as described above.

Tray Inoculation. Organisms were inoculated (100 μL volumes) using the BioMek FX robot. The final number of bacterial cells per well was approximately 2.5×10^4 CFU/mL. The inoculated trays were placed in stacks of no more than four and covered with an empty tray. The trays were incubated for 16–20 h at 35 $^\circ\text{C}$ in an ambient air incubator.

MIC Test Results. After inoculation and incubation, the degree of bacterial growth was estimated visually with the aid of a test reading mirror (Dynex Technologies 220–16) in a darkened room with a single light shining directly through the top of the microbroth tray. The MIC was the lowest concentration of drug which prevented macroscopically visible growth under the conditions of the test.

Determining the MIC_{90} . After all the MICs for each subset of strains were read, the values were sorted from highest to lowest and the MIC value where 90% of strains were inhibited at that value or below was considered the MIC_{90} .

Crystallization Procedure. LpxC protein was expressed and purified as previously described.¹⁵ Prior to crystallization, LpxC was diluted to a final concentration of 10 mg/mL in protein buffer with zinc chloride and ligand was added to 1 mM. The mixture was incubated at room temperature for 1 h before crystallization to allow for complex formation. Sitting drops composed of equal volumes of the LpxC/inhibitor complex and well solution were equilibrated over the well solution at 22 $^\circ\text{C}$. The crystals were grown in 0.1 M bis-tris pH 6.5, 0.1 M sodium citrate tribasic, 10 mM zinc chloride, 0.25 M guanidine HCl, and 28% polyethylene glycol 3350. Crystals were cryoprotected by quickly dipping them into well solution containing 16% ethylene glycol before flash-freezing them in liquid nitrogen.

X-ray diffraction data were collected at beamline 17-ID of the Advanced Photon Source facility. Structure refinement was carried out using the program BUSTER. The ligand was built into omit electron density after refinements with protein only, using the program COOT.

General Experimental. Starting materials, reagents, and solvents were purchased from commercial sources unless otherwise specified. NMR spectra were recorded on a Varian Unity 400 (available from Varian Inc., Palo Alto, CA) at room temperature and 400 MHz for proton. Chemical shifts are expressed in parts per million (δ) relative to residual solvent as an internal reference (acetonitrile- d_3) $\delta\text{H} = 1.94$ ppm and $\delta\text{C} = 1.32 \pm 0.02$ ppm, (chloroform- d) $\delta\text{H} = 7.26$ ppm and $\delta\text{C} = 77.16$ ppm, (dimethylsulfoxide- d_6) $\delta\text{H} = 2.50$ ppm and $\delta\text{C} = 39.52 \pm 0.06$ ppm, (methanol- d) $\delta\text{H} = 3.31$ ppm and $\delta\text{C} = 49.00$ ppm. The peak shapes are as denoted: s, singlet; d, doublet; dd, doublet of doublets; t, triplet; q, quartet; m, multiplet; br s, broad singlet. High-resolution mass spectrometry (HRMS) was collected on an Agilent (Wilmington, DE) 6220 Accurate Mass time-of-flight LC/MS operating in the electrospray ionization mode. The chromatography system consisted of an Agilent (Wilmington, DE) 1200 binary pumping system with the addition of an extra isocratic system and a dynamic splitter for dilution of samples as they passed between the UV detector and the mass spectrometer. The binary pump operated at 1.1 mL/min of A = 10 mM ammonium formate adjusted to pH 3.5 in water and B = 50:50 acetonitrile/methanol. Sample injections were typically 0.5 μL . Separations were effected using an Agilent (Wilmington, DE) Zorbax Eclipse Plus C-18 (3.0 mm \times 50 mm, 1.8 μm) column operating at 60 $^\circ\text{C}$. As samples eluted the UV detector, they were diluted in the dynamic splitter with an isocratic pump flowing at 0.5 mL/min and using a solvent of 50:50 methanol/water. Samples were diluted by factors ranging from 33:1 to 100:1. Data was processed using the MassHunter software that was provided with the instrument. Normal phase chromatography was performed using Biotage Isolera One purification systems or CombiFlash companions (Teledyne Isco, Inc.) and commercially available prepacked silica columns from Biotage, LLC., Silicycle, Inc., and Varian, Inc. Reverse phase chromatography was performed using a Biotage Isolera One purification system and prepacked Varian Septra C18 columns or via preparatory HPLC using a Agilent 1100 preparatory HPLC instrument. The tested compounds were determined to be >95% pure via HPLC.

■ ASSOCIATED CONTENT

📄 Supporting Information

Experimental methods and synthetic procedures for all intermediates and final compounds. This material is available free of charge via the Internet at <http://pubs.acs.org>. Compound 17v will be available to purchase from Sigma-Aldrich, Tocris, and Toronto Research Chemicals.

Accession Codes

The RCSB PDB code for the cocrystal structure of compound 2a with LpxC is 3UHM.

■ AUTHOR INFORMATION

Corresponding Author

*Phone: (860) 686-9120. E-mail: justin.montgomery@pfizer.com.

■ REFERENCES

- (1) Cooper, M. A.; Shlaes, D. Fix the antibiotics pipeline. *Nature* **2011**, *472*, 32.
- (2) Rice, L. B. Federal funding for the study of antimicrobial resistance in nosocomial pathogens: no ESKAPE. *J. Infect. Dis.* **2008**, *197* (8), 1079–1081.
- (3) Rice, L. B. Progress and challenges in implementing the research on ESKAPE pathogens. *Infect. Control Hosp. Epidemiol.* **2010**, *31* (Suppl 1), S7–S10.

(4) Boucher, H. W.; Talbot, G. H.; Bradley, J. S.; Edwards, J. E.; Gilbert, D.; Rice, L. B.; Scheld, M.; Spellberg, B.; Bartlett, J. Bad bugs, no drugs: no ESKAPE! An update from the Infectious Diseases Society of America. *Clin. Infect. Dis.* **2009**, *48* (1), 1–12.

(5) Barb, A. W.; Zhou, P. Mechanism and inhibition of LpxC: an essential zinc-dependent deacetylase of bacterial lipid A synthesis. *Curr. Pharm. Biotechnol.* **2008**, *9* (1), 9–15.

(6) Pitout, J. D.; Laupland, K. B. Extended-spectrum beta-lactamase-producing Enterobacteriaceae: an emerging public health concern. *Lancet Infect. Dis.* **2008**, *8* (3), 159–166.

(7) Nordmann, P.; Cuzon, G.; Naas, T. The real threat of *Klebsiella pneumoniae* carbapenemase-producing bacteria. *Lancet Infect. Dis.* **2009**, *9* (4), 228–236.

(8) Sidjabat, H.; Nimmo, G. R.; Walsh, T. R.; Binotto, E.; Htin, A.; Hayashi, Y.; Li, J.; Nation, R. L.; George, N.; Paterson, D. L. Carbapenem resistance in *Klebsiella pneumoniae* due to the New Delhi metallo-beta-lactamase. *Clin. Infect. Dis.* **2011**, *52* (4), 481–484.

(9) (a) Onishi, H. R.; Pelak, B. A.; Gerckens, L. S.; Silver, L. L.; Kahan, F. M.; Chen, M. H.; Patchett, A. A.; Galloway, S. M.; Hyland, S. A.; Anderson, M. S.; Raetz, C. R. Antibacterial agents that inhibit lipid A biosynthesis. *Science* **1996**, *274* (5289), 980–982. (b) Jackman, J. E.; Fierke, C. A.; Tumej, L. N.; Pirrung, M.; Uchiyama, T.; Tahir, S. H.; Hindsgaul, O.; Raetz, C. R. H. Antibacterial agents that target lipid A biosynthesis in gram-negative bacteria: inhibition of diverse UDP-3-O-(R-3-hydroxymyristoyl)-N-acetylglucosamine deacetylases by substrate analogs containing zinc binding motifs. *J. Biol. Chem.* **2000**, *275* (15), 11002–11009. (c) Clements, J. M.; Coignard, F.; Johnson, I.; Chandler, S.; Palan, S.; Waller, A.; Wijkman, J.; Hunter, M. G. Antibacterial activities and characterization of novel inhibitors of LpxC. *Antimicrob. Agents Chemother.* **2002**, *46* (6), 1793–1799. (d) Kline, T.; Andersen, N. H.; Harwood, E. A.; Bowman, J.; Malanda, A.; Endsley, S.; Erwin, A. L.; Doyle, M.; Fong, S.; Harris, A. L.; Mendelsohn, B.; Mdluli, K.; Raetz, C. R. H.; Stover, C. K.; Witte, P. R.; Yabannavar, A.; Zhu, S. Potent, Novel in Vitro Inhibitors of the *Pseudomonas aeruginosa* Deacetylase LpxC. *J. Med. Chem.* **2002**, *45* (14), 3112–3129. (e) Pirrung, M. C.; Tumej, L. N.; Raetz, C. R. H.; Jackman, J. E.; Snehalatha, K.; McClerren, A. L.; Fierke, C. A.; Gantt, S. L.; Rusche, K. M. Inhibition of the Antibacterial Target UDP-(3-O-acyl)-N-acetylglucosamine Deacetylase (LpxC): Isoxazolone Zinc Amidase Inhibitors Bearing Diverse Metal Binding Groups. *J. Med. Chem.* **2002**, *45* (19), 4359–4370. (f) Anderson, N. H.; Bowman, J.; Erwin, A.; Harwood, E.; Kline, T.; Mdluli, K.; Ng, S.; Pfister, K. B.; Shawar, R.; Wagman, A.; Yabannavar, A. Preparation of amino acid derivatives as antibacterial agents. WO 2004062601, 2004; (g) McClerren, A. L.; Endsley, S.; Bowman, J. L.; Andersen, N. H.; Guan, Z.; Rudolph, J.; Raetz, C. R. H. A Slow, Tight-Binding Inhibitor of the Zinc-Dependent Deacetylase LpxC of Lipid A Biosynthesis with Antibiotic Activity Comparable to Ciprofloxacin. *Biochemistry (Moscow)* **2005**, *44* (50), 16574–16583. (h) Shin, H.; Gennadios, H. A.; Whittington, D. A.; Christianson, D. W. Amphipathic benzoic acid derivatives: synthesis and binding in the hydrophobic tunnel of the zinc deacetylase LpxC. *Bioorg. Med. Chem.* **2007**, *15* (7), 2617–2623. (i) Mansoor, U. F.; Reddy, P. A. P.; Siddiqui, M. A. Preparation of methylhydantoin derivatives for use as antimicrobial agents. WO 2008027466, 2008; (j) Takashima, H.; Yoshinaga, M.; Ushiki, Y.; Tsuruta, R.; Urabe, H.; Tanikawa, T.; Tanabe, K.; Baba, Y.; Yokotani, M.; Kawaguchi, Y.; Kotsubo, H.; Tsutsui, Y. Preparation of quinoline-4-carboxylic acid and naphthyridine-4-carboxylic acid derivatives as antibacterial agents. WO 2008105515, 2008; (k) Barb, A. W.; Leavy, T. M.; Robins, L. I.; Guan, Z.; Six, D. A.; Zhou, P.; Bertozzi, C. R.; Raetz, C. R. H. Uridine-based inhibitors as new leads for antibiotics targeting *Escherichia coli* LpxC. *Biochemistry (Moscow)* **2009**, *48* (14), 3068–3077. (l) Reddy, P. A. P.; Mansoor, U. F.; Siddiqui, M. A. Preparation of heterocyclic compounds as LpxC inhibitors for use as antibacterial agents. WO 2009158369, 2009; (m) Benenato, K. E.; Choy, A. L.; Hale, M. R.; Hill, P.; Marone, V.; Miller, M. Preparation of hydroxamic acid derivatives as Gram-negative antibacterial agents. WO 2010100475, 2010; (n) Mansoor, U. F.; Reddy, P. A.; Siddiqui, M. A. Preparation of urea derivatives as

antibacterial agents for treatment of diseases mediated by LpxC. WO 2010017060, 2010; (o) Takashima, H.; Suga, Y.; Urabe, H.; Tsuruta, R.; Kotsubo, H.; Oohori, R.; Kawaguchi, Y. Preparation of N-hydroxy-naphthyridinecarboxamides as LpxC inhibitors and antibacterial agents. WO 2010024356, 2010; (p) Liang, X.; Lee, C.-J.; Chen, X.; Chung, H. S.; Zeng, D.; Raetz, C. R. H.; Li, Y.; Zhou, P.; Toone, E. J. Syntheses, structures and antibiotic activities of LpxC inhibitors based on the diacetylene scaffold. *Bioorg. Med. Chem.* **2011**, *19* (2), 852–860. (q) Mansoor, U. F.; Vitharana, D.; Reddy Panduranga, A.; Daubaras Dayna, L.; McNicholas, P.; Orth, P.; Black, T.; Siddiqui, M. A. Design and synthesis of potent Gram-negative specific LpxC inhibitors. *Bioorg. Med. Chem. Lett.* **2011**, *21* (4), 1155–1161.

(10) Brown, M. F.; Reilly, U.; Abramite, J. A.; Arcari, J. T.; Oliver, R.; Barham, R. A.; Che, Y.; Chen, J. M.; Collantes, E. M.; Chung, S. W.; Desbonnet, C.; Doty, J.; Doroski, M.; Engtrakul, J. J.; Harris, T. M.; Huband, M.; Knafels, J.; Leach, K. L.; Liu, S.; Marfat, A.; Marra, A.; McElroy, E.; Melnick, M.; Menard, C. A.; Montgomery, J. I.; Mullins, L.; Noe, M. C.; O'Donnell, J.; Penzien, J.; Plummer, M. S.; Price, L. M.; Shanmugasundaram, V.; Thoma, C.; Uccello, D.; Warmus, J.; Wishka, D. G. Potent inhibitors of LpxC for the treatment of gram-negative infections. *J. Med. Chem.* **2012**, *55*, 914–923.

(11) Smith, D. A.; Di, L.; Kerns, E. H. The effect of plasma protein binding on in vivo efficacy: misconceptions in drug discovery. *Nature Rev. Drug Discovery* **2010**, *9* (12), 929–939.

(12) Benet, L. Z.; Hoener, B. A. Changes in plasma protein binding have little clinical relevance. *Clin. Pharmacol. Ther.* **2002**, *71* (3), 115–121.

(13) Leach, A. G.; Jones, H. D.; Cosgrove, D. A.; Kenny, P. W.; Ruston, L.; MacFaul, P.; Wood, J. M.; Colclough, N.; Law, B. Matched molecular pairs as a guide in the optimization of pharmaceutical properties; a study of aqueous solubility, plasma protein binding and oral exposure. *J. Med. Chem.* **2006**, *49* (23), 6672–6682.

(14) Langsdorf, E. F.; Malikzay, A.; Lamarr, W. A.; Daubaras, D.; Kravec, C.; Zhang, R.; Hart, R.; Monsma, F.; Black, T.; Ozbal, C. C.; Miesel, L.; Lunn, C. A. Screening for antibacterial inhibitors of the UDP-3-O-(R-3-hydroxymyristoyl)-N-acetylglucosamine deacetylase (LpxC) using a high-throughput mass spectrometry assay. *J. Biomol. Screening* **2010**, *15* (1), 52–61.

(15) Mochalkin, I.; Knafels, J. D.; Lightle, S. Crystal Structure of LpxC from *Pseudomonas aeruginosa* complexed with the potent BB-78485 inhibitor. *Protein Sci.* **2008**, *17*, 450–457.